Available online at www.sciencedirect.com
ScienceDirect
Journal of Computational Physics xxx (2007) xxx–xxx
JOURNAL OF COMPUTATIONAL PHYSICS
www.elsevier.com/locate/jcp

Three-dimensional numerical investigation of a droplet impinging normally onto a wall film

N. Nikolopoulos [a], A. Theodorakakos [b], G. Bergeles [a,*]

[a] Department of Mechanical Engineering, Nat. Technical University of Athens, 15740 Zografos, Greece
[b] Fluid Research Co., H. Trikoupi 25, Athens, 10681, Greece

Received 9 December 2005; received in revised form 5 October 2006; accepted 2 December 2006

Abstract

The paper presents a three-dimensional numerical investigation of a droplet impinging normally onto a wall film. The numerical method is based on the finite volume solution of the Navier–Stokes equations coupled with the volume of fluid method (VOF) and utilizing an adaptive local grid refinement technique for tracking more accurately the liquid–gas interface. The results are compared with available experimental data for integral quantities such as the lamella temporal development. Two mechanisms are identified leading to secondary droplet formation; in the initial and intermediate stages of splashing secondary droplet formation is according to Rayleigh instability while at later times surface tension effects contribute further to secondary atomization. Moreover, the influence of Weber number on the impingement process is investigated and correlations for the diameter and number of secondary droplets are proposed.

Keywords: Deposition; Splashing; Lamella; Liquid film; Volume of fluid method

1. Introduction

The normal impact of a droplet onto a liquid film is a process occurring in many cases of engineering interest, such as fuel direct injection into internal combustion engines, surface cooling by water sprays, inkjet printing, as well as in a number of other physical processes realized in nature, for example the impact of raindrop onto the ground, which enhances soil erosion and produces secondary droplets that can act as carriers of spores and bacteria.

This complicated fluid mechanics phenomenon, is characterized by non-dimensional parameters as the droplet Weber number (We), the Reynolds number (Re), the Froude number (Fr) and the non-dimensional film thickness (H). Finally, a non-dimensional time (T) is also introduced. These parameters are defined as

* Corresponding author. Tel.: +30 2107721058; fax: +30 2107723616.
E-mail addresses: niknik@fluid.mech.ntua.gr (N. Nikolopoulos), andreas@fluid-research.com (A. Theodorakakos), bergeles@fluid.mech.ntua.gr (G. Bergeles).

0021-9991/$ - see front matter © 2006 Elsevier Inc. All rights reserved.
doi:10.1016/j.jcp.2006.12.002

$$We = \frac{\rho_2 D_o U_o^2}{\sigma}, \quad Re = \frac{\rho_2 D_o U_o}{\mu_2}, \quad Fr = \frac{U_o^2}{g \cdot h}, \quad H = \frac{h}{D_o}, \quad T = \frac{t U_o}{D_o} \tag{1}$$

where D_o and U_o are the diameter and mean impact velocity of the droplet, σ is the coefficient of surface tension, ρ_2, μ_2 are the density and dynamic viscosity of the liquid phase, g is the acceleration of gravity, h is the film height and t is time.

During the droplet impact onto a wall liquid film, the normal to the wall velocity component changes within a very short distance from that of the impinging droplet U_o (almost at the surface of the liquid film) to zero. This almost step-like jump in velocity in an incompressible liquid with a free surface, inevitably results in a liquid sheet out flowing normally to the free surface called lamella. During the lamella development, two main driving opposing forces influence its evolution, the inertia forces, which tend to stretch out the lamella and the surface tension forces, which tend to shrink the lamella. Accordingly, dominance of the surface tension effects over the inertial ones precludes the formation of three-dimensional structures, as fingering on the crown. Moreover inertial forces are damped by the viscous ones.

Weiss and Yarin [1] indicate that fingering occurs at the tip of the lamella formed at the limit of relatively weak surface tension (relative to the inertial effects, high *We* number), whereas sufficiently strong surface tension is able to suppress it (low *We* number).

The formation of the liquid sheet and its velocity were theoretically analyzed in the case of impact on a wetted solid surface by Yarin and Weiss [2]. In their analysis the evolution of the liquid sheet crown diameter generated by the impact of a drop on a liquid film, is expressed as

$$D(T) = C \cdot D_o \cdot (T - T_o)^n, \; n = 0.5, \quad C = \left(\frac{2}{3H}\right)^{0.25}, \tag{2}$$

where $D(T)$ is the crown diameter and n is a constant. The value of the constant C mainly depends on film thickness but the experiments reported by Cossali et al. [3] suggest a dependence also on the drop impact Weber number. The value of T_o can be also evaluated by a best fit procedure after n and C have been derived and ranges between 0 and 1.5. Fig. 1(a) and (b) show a typical form of a droplet during impingement and some basic global quantities concerning the lamella's dimensions; these quantities have been the subject of numerous investigations in the open literature.

The lamella temporal development depends on the parameters of the impact. Liquid jets may protrude from the crown, a process known as fingering, which subsequently may break-up to form secondary droplets. This is the well-known splashing regime realized with high impact *We* numbers, as reported by Levin and Hobbs [4], Macklin and Metaxas [5], Cossali, Coghe and Marengo [6], Wang and Chen [7]. For low impact

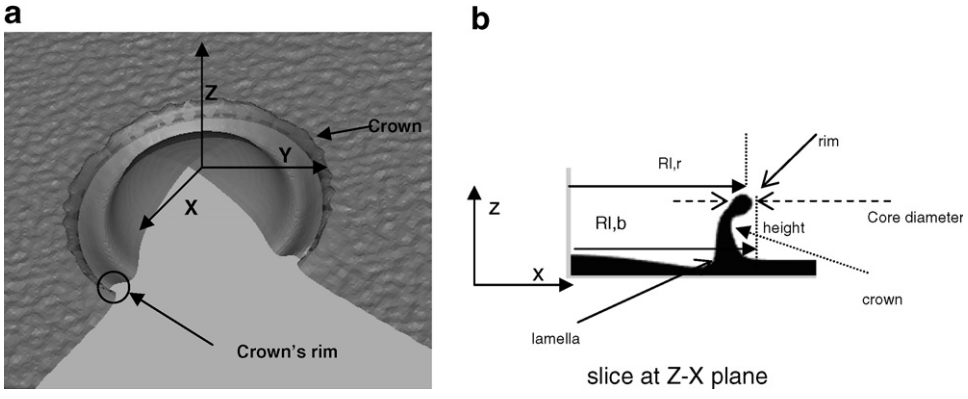

Fig. 1. Definition of impingement characteristics (droplet moves along the *Z*-axis, impinging onto the film on the *XY* plane): (a) Crown and crown's rim (perspective view); (b) some global quantities concerning the crown and lamella dimensions.

Please cite this article in press as: N. Nikolopoulos et al., Three-dimensional numerical investigation of a ..., J. Comput. Phys. (2007), doi:10.1016/j.jcp.2006.12.002

We numbers, the liquid sheet of the lamella may deposit on the wall film without any secondary droplet formation, creating capillary waves.

Yarin and Weiss [2] used an axisymmetric boundary method based on the integral equation for the scalar velocity potential imposing a discontinuity in the velocity distribution at the surface of the liquid layer on the wall. This results in the emergence of a liquid sheet normal to the film on the wall, propagating with the discontinuity. Surface tension and gravity were taken into account, whereas viscosity and compressibility were neglected. The splashing threshold is found as a function of the impact parameters, while analytical solutions for the crown's (rim's) tip velocity and the crown radius are produced. Roisman and Tropea [8] generalized this theory to the non-axisymmetric case for high *We* number impacts. The dynamic equations of motion of the crown are determined following a Lagrangian approach; therefore an analytical solution for the crown shape is formulated, in the asymptotic case that the surface tension and viscosity effects are negligible in comparison with inertial effects. Trujillo and Lee [9] extended Yarin and Weiss concept [2] for the propagation of kinematic discontinuity, including viscosity effects on the flow resulting from impact, i.e. the internal flow that moves liquid into the crown. Viscous effects seem to play an important role, some time after crown formation and not in the early stages, as also reported by Nikolopoulos et al. [10]. This indicates that in the case of high impact velocities the main influencing factor on the formation of the crown is the inertia of the liquid, while film thickness is more important for the crown radius evolution, as reported by Roisman and Tropea [8] and Trujillo and Lee [9].

Josserand and Zaleski [11] assuming potential flow matched to a small viscous region at the impact neck, proposed a theory predicting the transition between splashing and deposition for such kind of impinging events. Their theory is also based on the assumption that most of the liquid layer and the impacting droplet are unperturbed. This theory agrees both with recent experimental observations, such as those reported by Thoroddsen [12] and by numerical simulations using the VOF methodology and also presented in the same article.

For high *We* number impacts, liquid jets (fingering) originate at the crown rim of the lamella and subsequently break-up to form secondary droplets, as also verified from the present numerical investigation. The photographs of Levin and Hobbs [4], Stow and Hadfield [13], Yarin and Weiss [2], and Cossali et al. [6], clearly show that the formation of secondary droplets begins from cusps on the free rim. Later a thin jet originates from the cusp, which breaks up into secondary droplets, Yarin [14].

At first sight, the instability of the crown's rim might be explained by considering the rim as a toroidal cylinder, subject to capillary instability due to the growth of longitudinal perturbations leading to a reduction of its surface area and breakup. This mechanism is similar to the capillary breakup of thin free jets reported by Rayleigh [15]. However, according to Yarin and Weiss [2] this mechanism does not seem to explain the experimental data and they proposed a theory which connects the number of jets with the form of the initial perturbations in the very early phase of the impact, for example a small rippling of the liquid film or wall roughness.

Following Yarin and Weiss [2] work, Roisman and Tropea [8] explained the rim instability and formation of jets by considering small perturbations on the rim, which propagate with a velocity given by the Taylor theory [16] for a free liquid film of uniform thickness and constant velocity.

Rieber and Frohn [17] investigated this rim instability by solving numerically the Navier–Stokes equations for incompressible fluid in three dimensions. They used the volume of fluid method (VOF) of Hirt and Nichols [18] for tracking the liquid–gas interface. In order to get instabilities in the crown's rim and thus secondary droplets, they introduced a random disturbance with Gaussian distribution to the initial velocities of film and droplet, while the droplet shape was spherical. The standard deviation of the disturbance was chosen to be rather high, up to 0.5 U_o. Their conclusion was that the Rayleigh instability applies only to the formation of cusps at intermediate times after impact but not at the early stages.

Gueyffier and Zaleski [19] suggested another mechanism for the formation of jets in the very early phase of the impact depending on Richtmyer's [20] theory, which is linked to the sudden acceleration of the interface. In contrast with the approach of Rieber and Frohn [17] the initial spherical droplet shape had small harmonic perturbations and a uniform velocity profile; with these assumptions they were able to produce fingering.

Numerous numerical and experimental studies on the macroscopic outcome of splashing realized with impingement of liquid sprays have been presented by Arcoumanis et al. [21], Bai and Gosman [22], Morton

Please cite this article in press as: N. Nikolopoulos et al., Three-dimensional numerical investigation of a ..., J. Comput. Phys. (2007), doi:10.1016/j.jcp.2006.12.002

et al. [23], Stanton and Rutland [24], Tropea and Marengo [25], Cossali et al. [3,6] and others. The present work is trying to extend the three-dimensional numerical approach of Rieber and Frohn [17] and Gueyffier and Zaleski [19], including viscous effects and focusing mainly on the mechanism of fingering which can be analysed in more detail due to the employed grid adaptive numerical method around the liquid–gas interface.

2. Mathematical formulation

For a droplet splashing onto a wall film, a 2-D axis-symmetric numerical solution using the VOF methodology has been successfully applied in the past by the same authors, and described in more detail by Nikolopoulos et al. [10]. Here, the method has been extended to fully three-dimensional computations. The flow induced by the normal impingement of a droplet onto a wall is considered incompressible and laminar; the two-phase flow (phase 2 is the liquid phase, i.e. the droplet and the liquid film, phase 1 is the surrounding gas phase) is mathematically expressed by the Navier–Stokes equations and the continuity equation with extra terms taking into account the surface tension forces. For identifying each phase separately, the volume fraction, denoted by α, is introduced following the volume of fluid method (VOF) of Hirt and Nichols [18] defined as:

$$\alpha = \frac{\text{Volume of liquid phase}}{\text{Total volume of the control volume}} \tag{3}$$

The values of density and viscosity are calculated using linear interpolation between the values of the two phases weighted with the volume fraction α

$$\begin{aligned} \rho &= \alpha\rho_2 + (1-\alpha)\rho_1 \\ \mu &= \alpha\mu_2 + (1-\alpha)\mu_1 \end{aligned} \tag{4}$$

where the α-function is equal to:

$$a(x,t) = \begin{cases} 1, & \text{for a point } (x,t) \text{ inside liquid phase} \\ 0, & \text{for a point } (x,t) \text{ inside gas phase} \\ 0 < \alpha < 1, & \text{for a point } (x,t) \text{ inside the} \\ & \text{transitional area between the two phases} \end{cases} \tag{5}$$

The momentum conservation equation for both phases is written in the form

$$\frac{\partial(\rho\vec{u})}{\partial t} + \nabla\cdot(\rho\vec{u}\otimes\vec{u} - \vec{T}) = \rho\vec{g} + \vec{f}_\sigma \tag{6}$$

where $\vec{T}$ is the stress tensor, $\vec{u}$ is the velocity and f_σ is the volumetric force due to surface tension. The value of f_σ is equal to $f_\sigma = \sigma\cdot\kappa\cdot(\nabla a)$, where σ is surface tension (for immiscible fluids the value is always positive) and κ is the curvature of the interface region.

3. The numerical solution procedure

The governing Navier–Stokes conservation equations of the flow field are numerically solved on three-dimensional unstructured grids, following the finite volume approximation. Hexahedral computational cells are employed here. A recently developed adaptive local grid refinement technique of Theodorakakos and Bergeles [26] is also utilised in order to enhance accuracy of the predictions in the areas of interest (i.e the liquid–gas interface), with minimum computational cost. This is achieved by having relatively fine grid resolution at the regions of interest, and a coarse grid density where flow variable gradients are small. The solution procedure follows the SIMPLE algorithm of Patankar and Spalding [27]. In order to avoid pressure–velocity decoupling problems, the convective flux through each cell phase is calculated using the modifications of Rhie and Chow [28]. The volume of fluid method (VOF) of Hirt and Nichols [18] is used in order to track the gas–liquid interface.

Please cite this article in press as: N. Nikolopoulos et al., Three-dimensional numerical investigation of a ..., J. Comput. Phys. (2007), doi:10.1016/j.jcp.2006.12.002

To account for the high flow gradients near the interface, the computational cells are subdivided to the maximum resolution level with a user-prescribed number of layers in either side of the interface. As a result, the interface always lies inside the finest grid resolution. A new locally refined mesh is created every 20 time steps for the cases that will be presented afterwards. The computational cells where subdivision is performed are refined by a factor of 2 in every x–y–z direction, i.e in three dimensions the initial cell is split into eight. In that way a new grid with 1 level of local refinement is created. In the cases to be presented here, three levels of adaptive grid refinement are used, resulting in a very dense grid resolution in the regions of interest. Obviously, computations are more time efficient on the present dynamically adaptive grid, than on the equivalent fine resolution uniform grid.

The high-resolution CICSAM differencing scheme, which treats the whole gas–liquid domain as a single fluid system with variable density and viscosity as proposed by Ubbink and Issa [29] in the transport equation for α (VOF-variable) is used. The discretization of the convection terms of the velocity components is based on a high resolution convection-diffusion differencing scheme (Gamma scheme) proposed by Jasak [30]. The time derivative was discretized using the Crank–Nicolson second-order differencing scheme.

4. Numerical details

The flow domain is three-dimensional (Z-axis is opposite to the direction of gravity), the liquid phase is water and the gas phase surrounding the droplet was air under atmospheric pressure; isothermal impact of $T = 23\,^{\circ}\mathrm{C}$ has been assumed in all cases examined. The range of parameters for which computations have been performed are listed in Table 1.

For all cases the ''base'' grid employed consisted of 8000 cells. Three levels of local refinement are used, resulting to a maximum number of 417,000 computational cells. If a uniform fine grid were used, the number of cells that would be required in order to have the same resolution at the liquid–gas interface would be 4,095,638. The numerical simulation for case C of Table 1 has lasted for 25 days on a Pentium 4 with 2.4 GHz processor, while for case A computations last for 15 days, since the extent of lamella in case A is shorter than in case C and no secondary droplets are formed. At the start of calculations after grid refinement, the droplet and liquid film are discretised using 6044 and 128,000 cells, respectively.

Cases B and C are identical to those previously studied by Rieber and Frohn [17] using a 3-D approach with an equidistant Cartesian mesh in a rectangular computational domain covering a space of $X_{\mathrm{tot}} = 4D_{\mathrm{o}}$, $Y_{\mathrm{tot}} = 4D_{\mathrm{o}}$ and $Z_{\mathrm{tot}} = 4D_{\mathrm{o}}$ in the X, Y, Z dimensions, respectively. As a result the maximum refinement corresponds to a cell size of $D_{\mathrm{o}}/40$. In order to investigate the grid dependency of the results, cases B and C were also simulated with four levels of local refinement, resulting in a minimum cell size equal to $D_{\mathrm{o}}/80$. Implementing four levels of local refinement, the maximum number of used computational cells was around 1.5×10^6 (instead of 457,000 computational cells for three levels of local refinement). If a uniform fine grid were used, the number of cells that would be required in order to have the same resolution at the liquid–gas interface would be 32.5×10^6 (instead of 4,095,638 for three levels of local refinement). Due to computational time limitations, it was impossible to simulate the whole evolution of the phenomenon for cases B and C, just as it was attained using three levels of local refinement. The simulation of cases B and C using four levels of local refinement was performed until dimensionless time of $T = 1.85$ and $T = 3.15$, respectively, and has last for 30 days. Comparison of the results obtained for three and four levels of local refinement reveals any influence of mesh discretization on the accuracy of the simulation, as it will be shown later.

Plane $Z = 0.0$ is the bottom surface of the liquid film on the wall. Along the bottom of the computational domain, a static contact angle of 60° is imposed, whenever a triple phase of wall-gas and liquid is calculated. In

Table 1
The test cases examined

Case	We	Re	H	K	Dimensions of solution domain	Initial nodes (base grid)
A	125	7986	0.116	1732	$3.98D_{\mathrm{o}} \times 3.98D_{\mathrm{o}} \times 3.98D_{\mathrm{o}}$	$20 \times 20 \times 20$
B	250	11294	0.116	3463	$3.98D_{\mathrm{o}} \times 3.98D_{\mathrm{o}} \times 3.98D_{\mathrm{o}}$	$20 \times 20 \times 20$
C	598	17467	0.116	8284	$3.98D_{\mathrm{o}} \times 3.98D_{\mathrm{o}} \times 3.98D_{\mathrm{o}}$	$20 \times 20 \times 20$

Please cite this article in press as: N. Nikolopoulos et al., Three-dimensional numerical investigation of a ..., J. Comput. Phys. (2007), doi:10.1016/j.jcp.2006.12.002

addition, mirror boundary conditions that allow simulation of a droplet on the axis $X = Y = 0$ with fourfold symmetry are introduced. *We* number was varied by changing the initial velocity of the droplet.

The results which will be shown here have been obtained without introducing any disturbance either in the initial droplet velocity or to the droplet shape as Rieber and Frohn [17] or Gueyffier and Zaleski [19] were obliged to introduce into their solution procedure in order to predict secondary droplet formation.

The droplet is initially located around 2.8 diameters above the film surface, with a uniform initial velocity U_o. As a result, disturbances either on the surface shape or to the velocity field arise during the interaction of the droplet with the gas phase just before or during impact. A typical droplet shape with the corresponding numerical grid just before impact for case A, is shown in Fig. 2(a). The droplet has taken an oval shape with elongated radii by 1.2% D_o in the Z direction and shorten by 0.8% R_o in the X–Y directions, whilst a velocity wake has been formed behind it as shown in Fig. 2(b). It should be mentioned that the oval shape of the droplet changes with the impact velocity. For instance, in case B the oval droplet shape increases by 0.5% D_o in the Z direction and by 0.7% R_o in the X–Y-direction, whilst in case C, reduces by 1.5% D_o in the Z-direction and increases by 0.8% R_o in the X–Y-directions. Also and although the grid resolution is not adequate to fully resolve them, perturbations in form of capillary waves can be seen in Fig. 2(c) on the surface of the film.

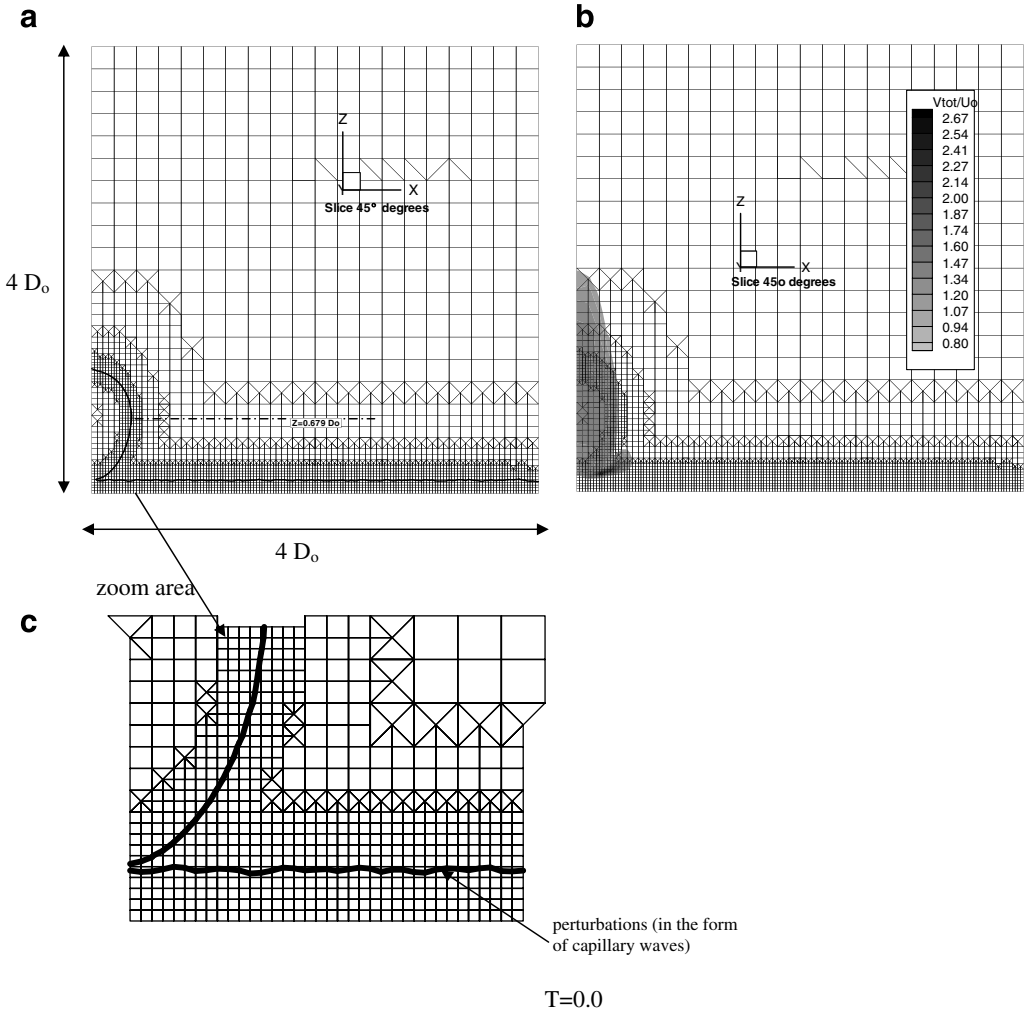

Fig. 2. (a) The droplet shape; (b) the contour of total velocity with the corresponding numerical grid just before the impact (slice 45° – $Z = 0.679D_o$); (c) perturbations in the form of capillary waves on the surface of the film.

Please cite this article in press as: N. Nikolopoulos et al., Three-dimensional numerical investigation of a ..., J. Comput. Phys. (2007), doi:10.1016/j.jcp.2006.12.002

5. Presentation and discussion of the results

5.1. Droplet deposition (case A, three levels of local refinement (locref = 3))

Yarin and Weiss [2] and Cossali et al. [6] determined the critical *We* number separating the post-impingement flow regime between deposition and splashing. A value of around $We = 200$ was found for the values of *Ohnesorge number* ($Oh = \mu_2/(\sigma\rho_2 D_o)^{1/2}$) and H considered in the present numerical investigation. Weiss and Yarin [1] found that the critical Weber number for crown formation is $We_c^{(crown)}$ around 100 for $H = 0.125$. These are confirmed by the present numerical simulation as the present predictions ($We = 125$) indicate crown formation and deposition. Fig. 3 indicates the predicted crown formation and velocity field at various times; a crown is formed with maximum height $D_o/2$ at $T = 2$, whose further development is constrained by surface tension forces and finally is deposited on the film and transformed to a surface wave, which can be seen in Fig. 3(a) at time $T = 5.586$.

During the initial stages of impact, the induced gas velocity field around the impacting droplet is characterized by a vortex ring attached to the crown's rim. This can be seen in Fig. 3(b) on the 45° slice plotted at $T = 0.611$. Parallel to the film surface area and outside the region of the crater, the gas jet initially formed in

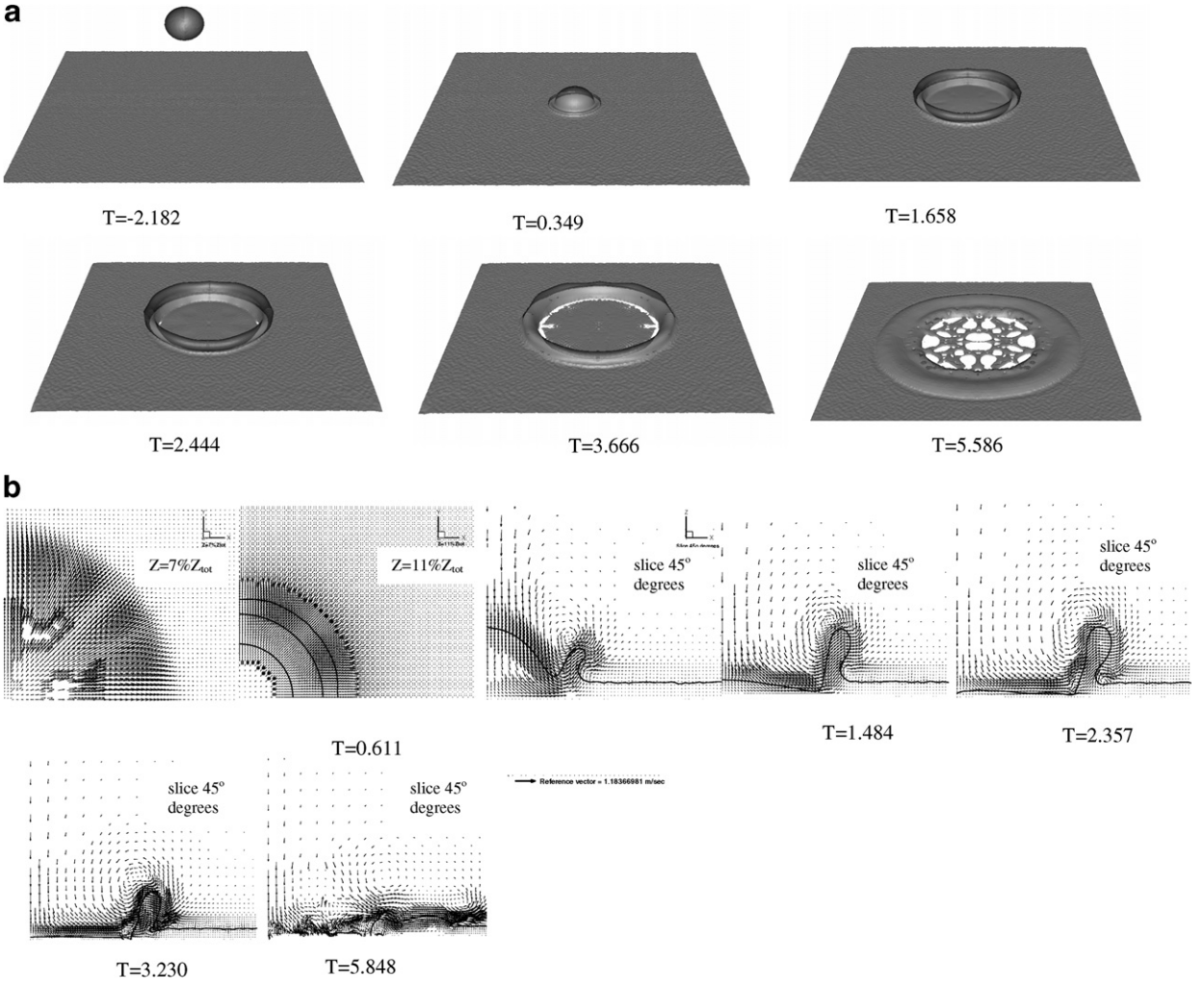

Fig. 3. (a) Time evolution of the impinging process for case A, (b) velocity field for case A at different slices ($We = 125$, $Re = 7986$, $H = 0.116$, $Fr = 182$, locref = 3).

Please cite this article in press as: N. Nikolopoulos et al., Three-dimensional numerical investigation of a ..., J. Comput. Phys. (2007), doi:10.1016/j.jcp.2006.12.002

the space between the droplet and the liquid surface ($T = 0.0$) is maintained and its velocity increases, getting closer to the film surface. This can be seen in Fig. 3(b), at $T = 0.611$ on the $Z = 7\%\ Z_{tot}$, $Z = 11\%\ Z_{tot}$ horizontal slices. On the same plot, three-dimensional disturbances can be seen near the film surface. The liquid wall-jet is flowing against the motionless liquid film, which is pushed to lift off creating the observed liquid crown.

The crown traveling outwards, maintains contact with the wall-film through a thin liquid sheet, spreading radially outwards and also increasing its core diameter. A neck at the bottom of the crown, close to the film surface is also created but without breaking down to smaller fragments. As can be seen in Fig. 3(b) at time $T = 2.357$ the crown under the effect of surface tension and gravity starts to recede, until its full absorption by the remaining mass of film on the wall evident again on the same Fig. 3(b) at $T = 3.230$ on the 45° slice. During the life time of the crown evolution, a kidney-type vortex ring is attached to the upper region of the crown. The crown, after its collapse, mixes with the liquid forming the wall film and its kinetic energy is transformed to a surface wave moving outward of the crater. According to model predictions, the transport (radial) velocity of this wave is about 25% of the impact droplet velocity.

The value of the maximum gas velocity (at the region of the crown rim) is approximately 275% of the droplet impact velocity, whilst the maximum liquid velocity is approximately 177% of the initial droplet velocity. Values of the pressure coefficient C_p, defined here as $\Delta P/\frac{1}{2}\rho_2 U_o^2$, where ΔP is the difference of pressure from the atmospheric one, are estimated to be as high as 253% of the initial droplet kinetic energy at the front stagnation point during the initial stages of impact at $T = 0.0349$. Finally, Fig. 4 shows air bubbles entrapped between the droplet and the film, as has been also reported by Oguz and Prosperetti [31].

The radial distances at the rim $R_{l,r}$ and at the bottom $R_{l,b}$ of the spreading lamella, the core radius and the maximum height of lamella are calculated and shown in Fig. 5 as a function of time at the cross-section $Y = 0$. The predicted crown diameter is compared with the analytic expression of Yarin and Weiss [2] (“Eq. (2)”). The agreement between the two sets of predictions is very good, suggesting that the basic hydrodynamic characteristics of the spreading lamella are accurately predicted. It must also be noted that the lamella evolution up to a time $T = 3$ has almost an axi-symmetric form and after that time three-dimensional structures (mainly within the crater) start to appear, Fig. 3(a).

5.1.1. Droplet marginal splashing (case B, three levels of local refinement (locref = 3)*)*

The prediction of case B, which corresponds to an impact *We* number of 250, indicates marginal splashing, as it can be seen in Fig. 6(a) at $T = 5.431$. This is in qualitative agreement with the experimental findings of

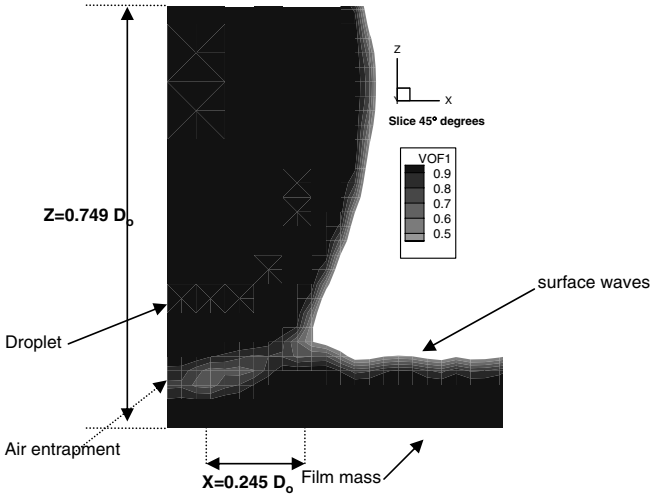

Fig. 4. VOF contour of the droplet–film interface at $T = 0.0349$.

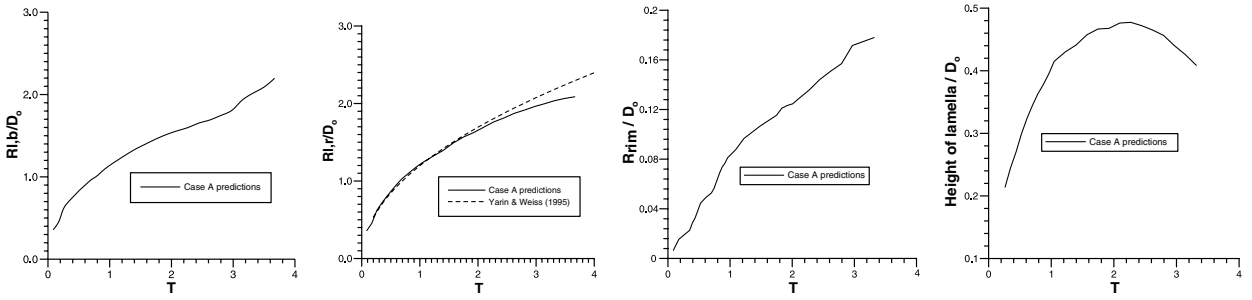

Fig. 5. Time evolution of lamella, case A, at $Y = 0.0$ ($We = 125$, $Re = 7986$, $H = 0.116$, $Fr = 182$, locref $= 3$).

Cossali et al. [6]. Rieber and Frohn [17] have predicted for the same case splashing and finger formation whilst the present simulation indicates a torus detachment and subsequent disintegration.

Fig. 6(a) shows that in the present predictions the crown rim maintains its contact with the lamella up to $T = 2.962$. Subsequently, the first ring detaches from the advancing crown similar to the 2-D axisymmetric calculations of Nikolopoulos et al. [10]. Instabilities on the surface and/or the flow field lead subsequently to the formation of ligaments, which further result into droplets at their ends, as shown at $T = 6.542$ in Fig. 6(a). The ring subsequently disintegrates into 16 relatively larger diameter droplets and eight smaller ones, shown at $T = 8.888$ of Fig. 6(a). At times between $T = 4.938$ and $T = 5.431$, a second ring almost detaches from the lamella but does not disintegrate. This second ring and the lamella subsequently merge with the wall film creating waves on the free liquid surface having a velocity of approximately 20% of the initial droplet velocity; these can be also seen in Fig. 6(a) and (c) at $T = 8.888$.

Fig. 6(c) indicates the induced velocity field at various time steps following the start of calculations at $T = 0.0$. The vortex ring created at the initial stages of impact is shown in Fig. 6(c) and it is attached to the tip of the crown at $T = 2.345$ on the 45° slice, while the detachment of the first ring from the crown is shown on the same figure at $T = 3.827$. After the disintegration into secondary droplets, the vortex ring weakens and around each secondary droplet two weak recirculation zones exist, and shown on the $Z = 21\%\ Z_{\text{tot}}$ slice of Fig. 6(c) at $T = 8.888$.

The predicted dimensions of the lamella are compared to various calculations reported in the literature for the same case. In particular, the 3-D numerical calculations of Rieber and Frohn [17] the analytic expression of Yarin and Weiss [2] which will be referred to as "Eq. (2)", and the numerical 2-D axisymmetric results of Nikolopoulos et al. [10] are included in Fig. 7 together with the present predictions. This graph indicates the development of lamella's height with time and the increase of the core radius, before its detachment from the advancing crown. The results indicate that up to a dimensionless time of $T = 3$ for which predictions from Rieber and Frohn [17] are available, good agreement with the present predictions exists.

5.1.2. Crown's dynamics

Wu [32] derived an approximate torus Weber number We_{r}, above which an expanding torus disintegrates into secondary droplets, under the assumption of Rayleigh instability. This Weber number (We_{r}) is defined as:

$$We_{\text{r}} = \frac{\rho_2 D_{\text{l}} U_{\text{l}}^2}{\sigma} \tag{7}$$

where D_{l} and U_{l} are the diameter and the velocity, respectively, of an equivalent droplet having the same mass and kinetic energy as that of the torus. It is assumed that the magnitude of the initial perturbations on the crown's rim is the same with that of the induced surface waves on the film surface. The amplitude of the capillary waves on the film surface relative to the diameter of the equivalent droplet $r_\alpha = 2\delta_{\text{o}}/d_{\text{l}}$ is of the order of $O[10^{-2}]$. According to Wu [32] the approximate critical We_{r} for the breakup of an expanding torus is given by $We_{\text{r}} = 22.48\ln^{2/3}(1/r_{\text{a}})$. For this wave amplitude a Weber number of the order of 60 is calculated. This theory is applied in the present case assuming that the crown rim becomes a torus, after detachment and calculating the average We_{r} number at different times.

Please cite this article in press as: N. Nikolopoulos et al., Three-dimensional numerical investigation of a ..., J. Comput. Phys. (2007), doi:10.1016/j.jcp.2006.12.002

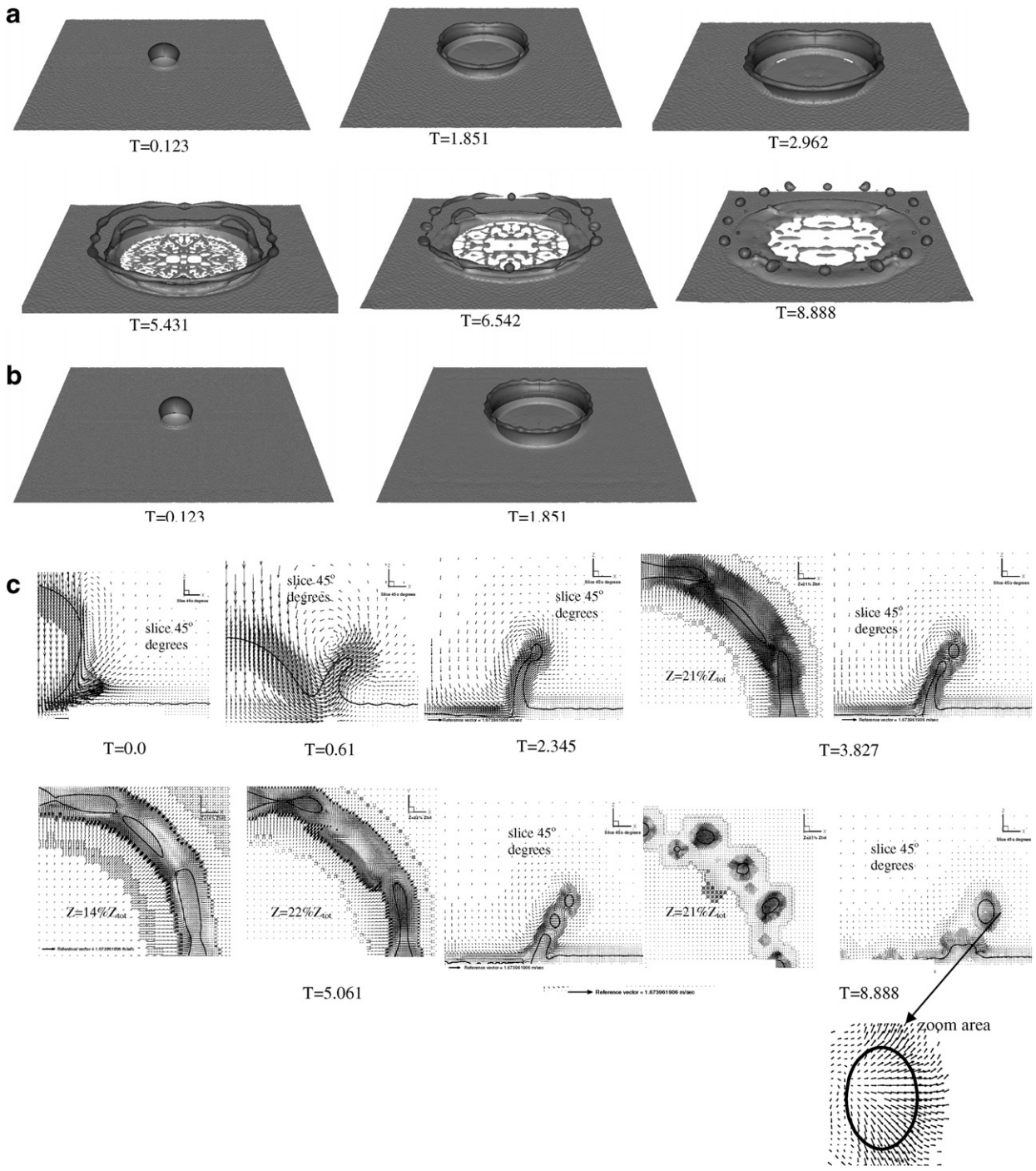

Fig. 6. (a) Time evolution of the impinging process for case B using three levels of local refinement; (b) time evolution of the impinging process for case B using four levels of local refinement; (c) velocity field for case B at different slices ($We = 250,\ Re = 11294,\ H = 0.116,\ Fr = 363,\ \text{locref} = 3$).

The local average *Weber* number of the detached rim, calculated at the slice of 45 of the computational domain, is given in Table 2 at various time steps. E_{sur} and E_{kin} are the surface and kinetic energy of the torus (tor) or the equivalent droplet (eq.diam), respectively. At about time $T = 2.839$, just before the first ring

Please cite this article in press as: N. Nikolopoulos et al., Three-dimensional numerical investigation of a ..., J. Comput. Phys. (2007), doi:10.1016/j.jcp.2006.12.002

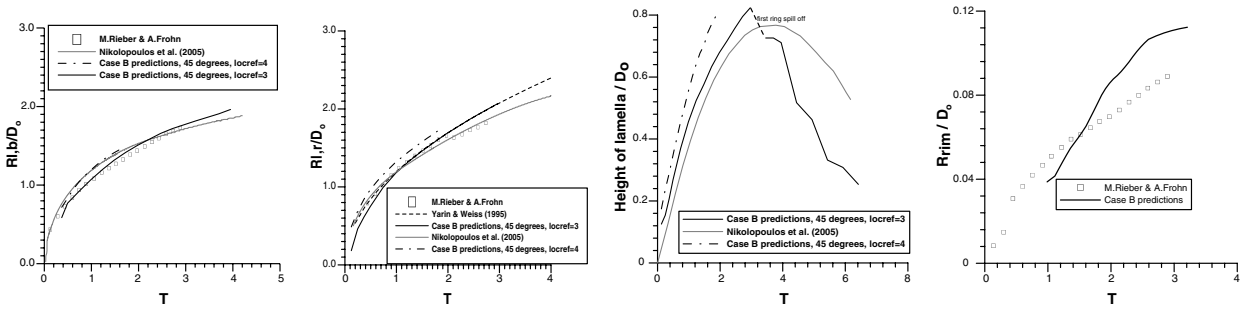

Fig. 7. Time evolution of lamella, case B ($We = 250,\ Re = 11294,\ H = 0.116,\ Fr = 363,\ \text{locref} = 3, 4$).

Table 2
Variables concerning the torus rim evolution for case B

T	d_{se}	d_c	U_{tor}	d_l	$E_{sur,tor}$	$E_{kin,tor}$	$E_{sur,eq.diam}$	$E_{kin,eq.diam}$	We_{crown}
2.839 (first ring, detached)	1.26E − 03	0.027	0.633	0.006	2.58E − 05	2.10E − 05	8.40E − 06	3.82E − 05	54.6
2.839 (second ring, not detached)	3.70E − 04	0.025	0.805	0.0025	7.02E − 06	2.70E − 06	1.56E − 06	8.16E − 06	62.6
3.456 (first ring, detached)	1.27E − 03	0.029	0.540	0.006	2.85E − 05	1.70E − 05	9.05E − 06	3.65E − 05	48.3
3.456 (second ring, not detached)	7.80E − 04	0.027	0.514	0.0043	1.59E − 05	5.30E − 06	4.45E − 06	1.67E − 05	45.2
4.197 (second ring, not detached)	1.26E − 03	0.029	0.387	0.006	2.78E − 05	8.40E − 06	8.84E − 06	2.74E − 05	37.2
5.308 (third ring, not detached)	1.71E − 03	0.003	0.309	0.0035	3.78E − 06	9.90E − 07	2.87E − 06	1.90E − 06	7.9

$We = 250,\ Re = 11294,\ H = 0.116,\ Fr = 363,\ \text{locref} = 3.$

detachment from the crown, the diameter of the equivalent droplet is $d_l = 0.006$ m. At this time, the We number of the detached ring is approximately 55, which is near to the critical Weber number for torus disintegration. Thus, this torus might break up into secondary droplets in a mechanism similar to Rayleigh instability. This is confirmed by the present numerical results.

At time $T = 2.839$, the mean value of the cross-sectional torus diameter is calculated to be $d_{se} = 1.26$ mm. The theoretical diameter of the secondary droplets, following Rayleigh instability theory should be equal to $d_{sec,drop} = 1.889 d_{se}$, which results to $d_{sec,drop} = 2.38014$ mm. The first spherical droplet's diameter at about time $T = 6.296$, to which the rim disintegrates, is found to be 2.459 mm (0.36 D_o), in close agreement with the theoretical value. The other droplets are of ligament type. The theoretical maximum wavelength of the most unstable wave is known to be equal to 4.55 d_{se}, i.e 5.642 mm. Therefore the theoretical number of the produced droplets is $\pi\ d_c/(4.55\ d_{se})$, i.e 15, a number which is in close agreement with the predicted one of 16.

5.1.3. Satellite droplets

The size of the secondary droplet was evaluated by image analysis of the top view pictures, using commercial software. This secondary droplet size distribution is calculated at two time instants corresponding to $T = 8.518$ and $T = 9.258$ after impact. At $T = 8.518$, six satellite droplets (four large diameters and two small diameters droplets) are formed in the 90° computational domain sector, which correspond to a total number of 24 for the full 360°. The smallest satellite droplet has a mean size, normalized with the initial droplet diameter D_o, equal to 0.136, the second one equal to 0.15, the third equal to 0.31, the fourth 0.39, the fifth 0.40 and the last one 0.42. At this time $T = 8.518$, the arithmetic mean diameter (AMD) of the satellite droplets has a value of 0.30 and at time $T = 9.258$, where five satellite droplets are visible, the mean value is 0.36. This increase in the value of AMD with time is due to coalescence between secondary droplets.

5.1.4. Grid dependency

In order to test the grid dependency of the results, prediction of case B, using four levels of local refinement has been undertaken. This simulation is in accordance with the corresponding one using three levels of local refinement, as far as the general evolution of the phenomenon is concerned, until dimensionless time $T = 1.85$,

Please cite this article in press as: N. Nikolopoulos et al., Three-dimensional numerical investigation of a ..., J. Comput. Phys. (2007), doi:10.1016/j.jcp.2006.12.002

Fig. 6(b), for which predictions have been obtained using a finer mesh. "Prompt" splashing is not observed and a torus detachment is again predicted (details not shown). Thus, the hydrodynamics does not seem to be significantly depend on the level of mesh refinement. In addition Fig. 7 presents also results for the finer mesh of the time evolution of the lamella's dimensions. As far as the lamella's dimensions are concerned, a good agreement between three and four levels of local refinement is found. Nevertheless, for the lamella's height an increase is predicted using four levels of local refinement (less than 15%), due to the more vertical lamella's growth. Moreover, this is combined with a smaller average crown's thickness.

The calculated maximum gas, liquid velocity and pressure at times $T < 0.036$ and $T > 0.086$ take almost the same values for three and four levels of local refinement. However, during the intermediate times ($0.036 < T < 0.086$) the predicted values begin to differ. For example the maximum gas and liquid velocity during this period are approximately 400% and 237%, respectively, of the droplet impact velocity; the maximum pressure value is approximately 328% of the initial droplet kinetic energy, in terms of C_p defined in section 5.1, at the front stagnation point. These peak values are about 40% higher compared to those obtained with three levels of local refinement.

5.1.5. Droplet splashing (case C, three levels of local refinement (locref = 3)*)*

Case C is the highest *We* number case, but for the same Ohnsesorge number and dimensionless film thickness. Under these conditions of impact, the experimental investigations by Cossali et al. [6] indicate that splashing occurs; this has been also verified by the present numerical results.

The evolution of splashing can be subdivided into four phases, whose characteristics can be observed through the different time instants of Fig. 8(a): (a) prompt splashing and crown formation, Fig. 8(a), $T = 2.004$, (b) rim cusping and jetting, Fig. 8(a), $T = 3.532$, (c) break-up of the jets and formation of secondary droplets Fig. 8(a), $T = 5.441$ and finally (d) crown collapsing, Fig. 8(a), $T = 7.541$. This stage evolution was also observed experimentally by Cossali et al. [6]. During the second phase, fingers which elongate and subsequently break up into secondary droplets are observed.

Fig. 8(c), shows the velocity vector distribution to planes parallel and normal at 45° to the film surface as a function of time. Just like in the previous cases, an air and a liquid jet are formed simultaneously, originated from the neck between the impinging droplet and the film. It is of interest to note that both the maximum non-dimensional pressure and the air and liquid velocity are about equal in all cases A, B and C, indicating the similarity of the impinging process at the initial stages of impact, independently of the *We* number.

Cossali et al. [6] mention that in the case of a low viscosity liquid, during the initial stages of lamella creation, secondary droplets are detaching from it. However, with high viscosity liquid, secondary droplets were observed to detach only after full development of the lamella's crown. In the low viscosity case droplets may still be detaching from jets even during the crown collapsing period. Thus, the viscosity appears to play an important role in defining the splash morphology and consequently the dynamic characteristics (size and velocity) of the secondary droplets. This is in conjunction with the numerical experiments of Nikolopoulos et al. [10] indicating that the viscosity of the liquid is influential in the later stages of splash evolution, when secondary droplets are on the verge of spill off due to the shear forces that are developing in the rim of lamella.

The predicted dimensions of the lamella are compared to the 3-D numerical calculations of Rieber and Frohn [17] to the analytic expression of "Eq. (2)" from Yarin and Weiss [2] and to the numerical results of Nikolopoulos et al. [10] in Fig. 9. The results indicate that up to a dimensionless time of $T = 3$, there is a very good agreement with the corresponding results from other researchers.

5.1.6. Number of jets and jet's growth (Fig. 10, three levels of local refinement (locref = 3)*)*

The instability of the rim creates a number of jets-fingers, which elongate with time and eventually break-up to yield the secondary droplets through a mechanism similar to the Rayleigh instability. Five stages of jetting occur in the present case and these can be seen in Fig. 10(b). From the simulation, it was possible to evaluate not only the number of jets produced, but also their elongation as a function of time. The evaluation of these two characteristics was based on the results at the middle sector of 37.22° of the computational domain. The first 48 jets (Fig. 10(a)), at the periphery of the crown appear at about time $T = 0.668$ and their number up to 1.7 ms does not change; then the number of jets up to time $T = 3.0$ increases, but afterwards this number decreases possibly due to the merging of the closest jets during the crown evolution, in contrast to the results

Please cite this article in press as: N. Nikolopoulos et al., Three-dimensional numerical investigation of a ..., J. Comput. Phys. (2007), doi:10.1016/j.jcp.2006.12.002

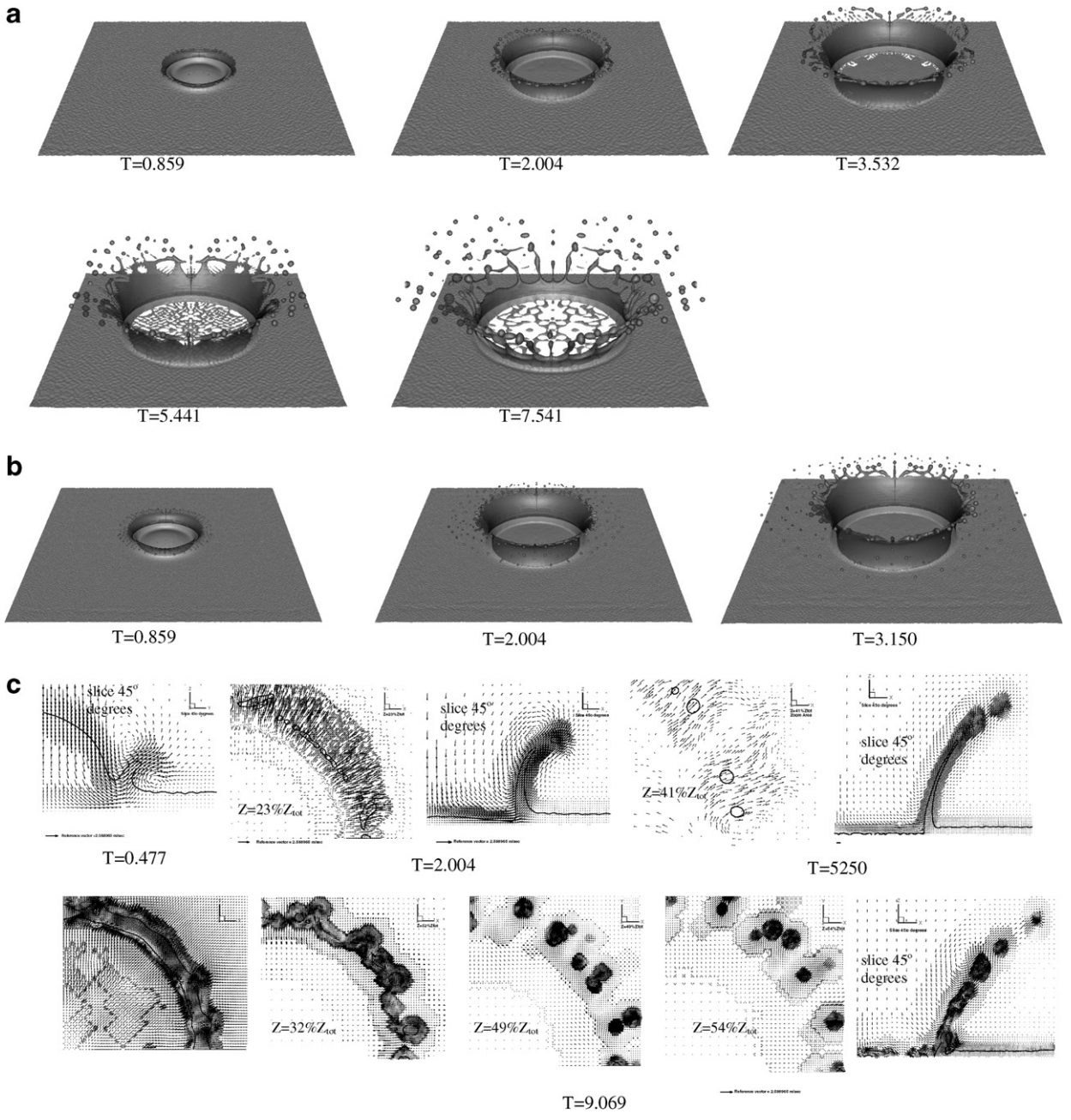

Fig. 8. (a) Time evolution of the impinging process for case C using three levels of local refinement; (b) time evolution of the impinging process for case C using four levels of local refinement; (c) velocity field for case C at different slices ($We = 598$, $Re = 17467$, $H = 0.116$, $Fr = 867$, locref $= 3$).

reported by other researchers, like Cossali et al. [6], Yarin and Weiss [2], who found that the number of jets monotonically decreases. However, using four levels of local refinement (Fig. 10(a)) the experimental finding is confirmed, indicating that the dynamics of "prompt" splashing depends on the mesh size. The jet elongation (L_j), Fig. 10(b), at which droplet spill-off occurs, for the first three jetting is almost constant and then decreases. The decrease of L_j with time suggests a decrease of the jet's diameter with time, which is supported by the numerical results, Table 3, and experimentally verified by Cossali et al. [6]. The liquid velocity of each jet at its middle and at the time of separation from the crown's rim is calculated and for the first jetting is

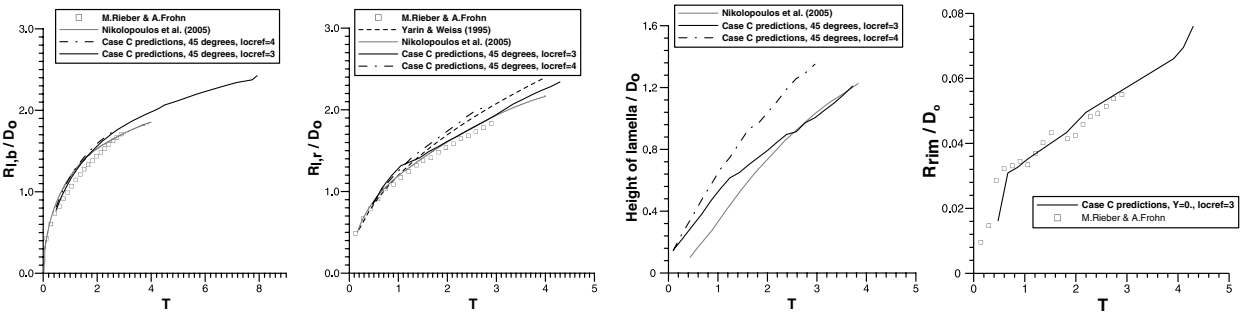

Fig. 9. Time evolution of lamella, case C ($We = 598,\ Re = 17467,\ H = 0.116,\ Fr = 867,\ \text{locref} = 3, 4$).

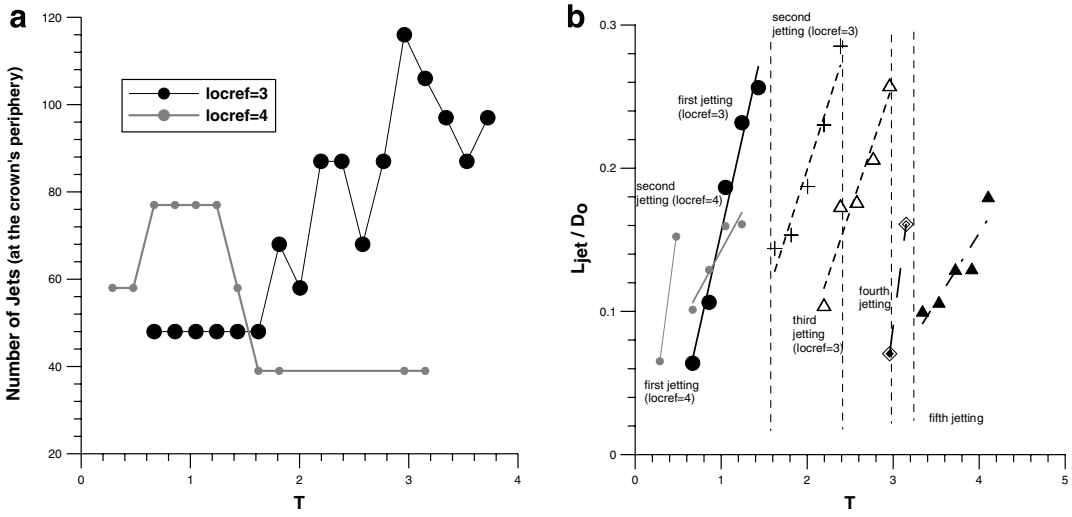

Fig. 10. (a) Number of jets; (b) their elongation as a function of time for case C, using three and four levels of local refinement ($We = 598,\ Re = 17467,\ H = 0.116,\ Fr = 867,\ \text{locref} = 3, 4$).

Table 3
Jet's elongation and its thickness for case C

Jetting	$D_{\text{jet}}/D_{\text{o}}$	$L_{\text{jet}}/D_{\text{o}}$
First	0.048	0.256
Second	0.037	0.285
Third	0.041	0.259
Fourth	0.029	0.161
Fifth	0.031	0.179

$We = 598,\ Re = 17467,\ H = 0.116,\ Fr = 867,\ \text{locref} = 3.$

approximately 0.5 m/s, for the second approximately 0.3 m/s, for the third approximately 0.4 m/s, for the fourth approximately 1 m/s and approximately 0.15 m/s for the last one.

5.1.7. Evolution of secondary droplet's diameter, just detaching from the jet, three levels of local refinement (locref = *3*)

If Rayleigh instability [15] is the mechanism leading to secondary droplets detaching from the jets, then the their diameter should be proportional to the jet diameter ($d_{\text{sec,droplet}} = 1.889 d_{\text{jet}}$). The sectional diameter of the

fingers is evaluated by the numerical data and is given for each case at different times in the corresponding tables. Thus calculating the size of only those droplets that are detaching each time from the jet, a direct comparison can be made, revealing to which extent these two diameters, the theoretical from Rayleigh instability and the predicted one, agree.

The theoretical Rayleigh's theory value of the mean secondary droplet diameter, normalised with the initial droplet diameter is given in Table 4. The mean secondary droplet is evaluated by the numerical results, in the region of the middle sector of 37.22° of the computational domain, and it is also given in Table 4. The comparison between these two values is given in Fig. 11(a); as can be seen, a good agreement is achieved. Thus, it can be concluded that Rayleigh instability is the dominant mechanism of splashing, not only at the intermediate stages of impingement, as reported by Rieber and Frohn [17] but also at the initial ones. The number of

Table 4
Mean secondary droplet diameter (just detaching from the jet) according to Rayleigh's theory and the corresponding calculated value from the numerical results as a function of time for case C

T	$d_{drop,sec}/D_o$ (Rayleigh, $1.889d_{jet}$)	$d_{drop,sec}/D_o$ (via numerical results)
1.241	0.079	0.102
1.432	0.051	0.078
1.623	0.070	0.054
2.005	0.053	0.053
2.387	0.054	0.055
2.768	0.054	0.056
2.959	0.055	0.051
3.341	0.059	0.055
3.723	0.060	0.080

$We = 598,\ Re = 17467,\ H = 0.116,\ Fr = 867,$ locref $= 3$.

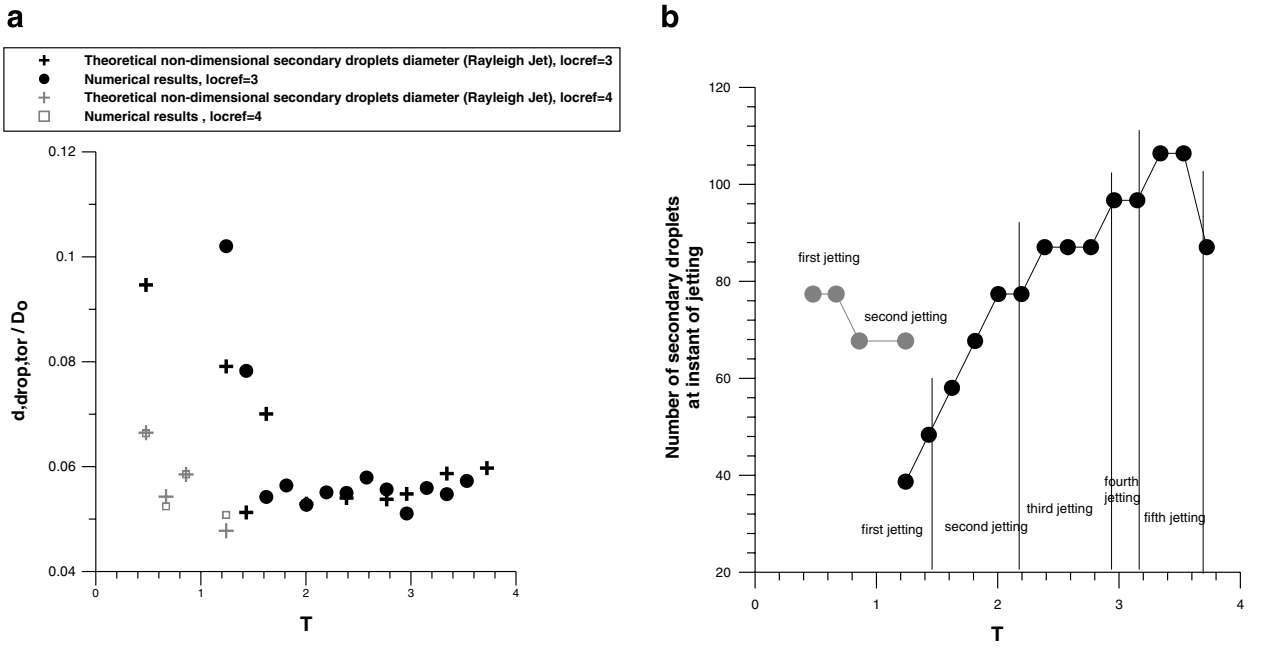

Fig. 11. (a) Mean secondary droplet diameter (just detaching from the jet) according to Rayleigh's theory and the corresponding value from the numerical results; (b) their number, as a function of time for case C, using three or four levels of local refinement ($We = 598,\ Re = 17467,\ H = 0.116,\ Fr = 867,$ locref $= 3, 4$).

Please cite this article in press as: N. Nikolopoulos et al., Three-dimensional numerical investigation of a ..., J. Comput. Phys. (2007), doi:10.1016/j.jcp.2006.12.002

the droplets, just detaching from the jets, converted from 37.22° sector to 360° is shown as a function of time in Fig. 11(b). It seems that the number of the produced droplets, increases up to time $T = 3.5$.

After, the beginning of the crown's collapse, due to surface tension effects, the number of secondary droplets formed, decreases, and another mechanism of breaking-up takes place. This mechanism depends on surface tension forces, and not on inertia. This increase of non-dimensional secondary droplet diameter was also reported by Cossali et al. [6].

5.1.8. Evolution of satellite droplet's diameter, three levels of local refinement (locref = *3*)

The satellite droplet's diameter was evaluated using the numerical results, at different time instants. Again, the middle sector of 37.22° of the computational domain was used as the reference domain of evaluation. The time evolution of the average mean diameter (AMD) is shown in Fig. 12(a). The dependence of mean droplet size with time can be expressed by a power law as proposed by both the theory of Yarin and Weiss [2] and the experimental work of Cossali et al. [6]. This empirical correlation can take the following form:

$$\frac{d_{\text{sec}}}{D_{\text{o}}} = qT^m \tag{8}$$

where the exponent m, according to theory is 1/2, and according to the experiments for $We = 484$ is equal to 0.43 and for $We = 667$ is equal to 0.56. For the We number of case C a best fit curve to the predictions gives an exponent of 0.502 for the whole evolution of the phenomenon. The number of droplets with time, shown in Fig. 12(b), indicates that it increases until time $T = 3.5$ and then decreases due to coalescence, with the simultaneous increase of secondary droplet size.

The size distribution of the secondary droplets at various times is presented in Fig. 13. During the initial stages of jetting, this distribution of satellite droplets is narrow, but later the distribution is wider, $T = 7.3506$. After the crown's collapse, bigger than in the beginning of jetting, satellite droplets are produced, whilst coalescence between droplets takes place.

5.1.9. Crown's dynamics

After the crown is formed, it begins to increase in diameter and height, with reduced width. During its outwards movement, two types of wave perturbations are visible. The first one is in the longitudinal direc-

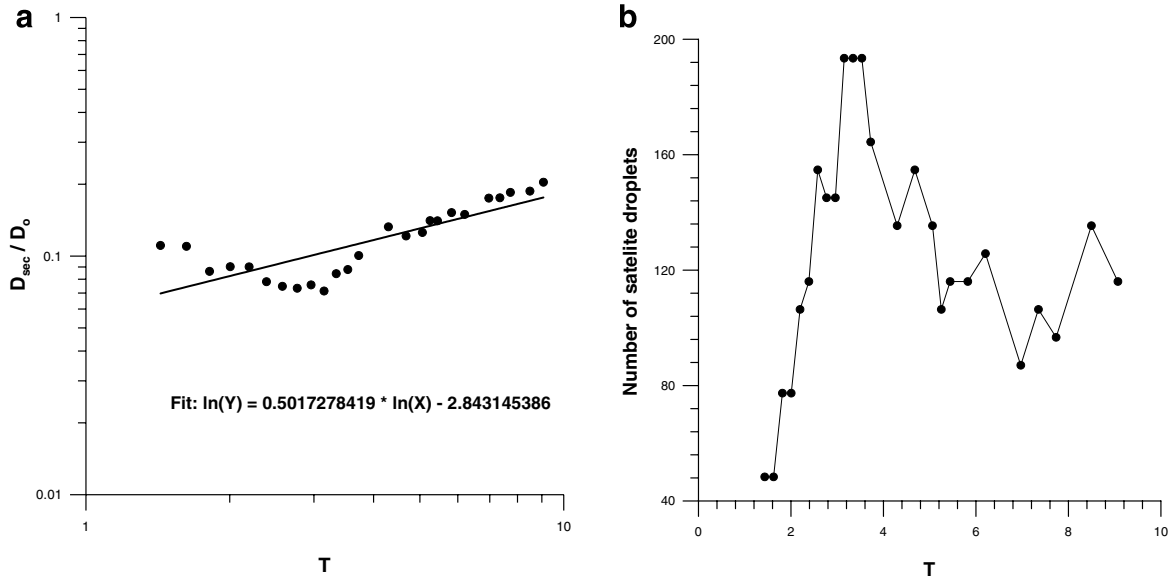

Fig. 12. (a) Mean satellite droplet diameter; (b) droplet number, as a function of time for case C, using three levels of local refinement ($We = 598$, $Re = 17467$, $H = 0.116$, $Fr = 867$, locref = 3).

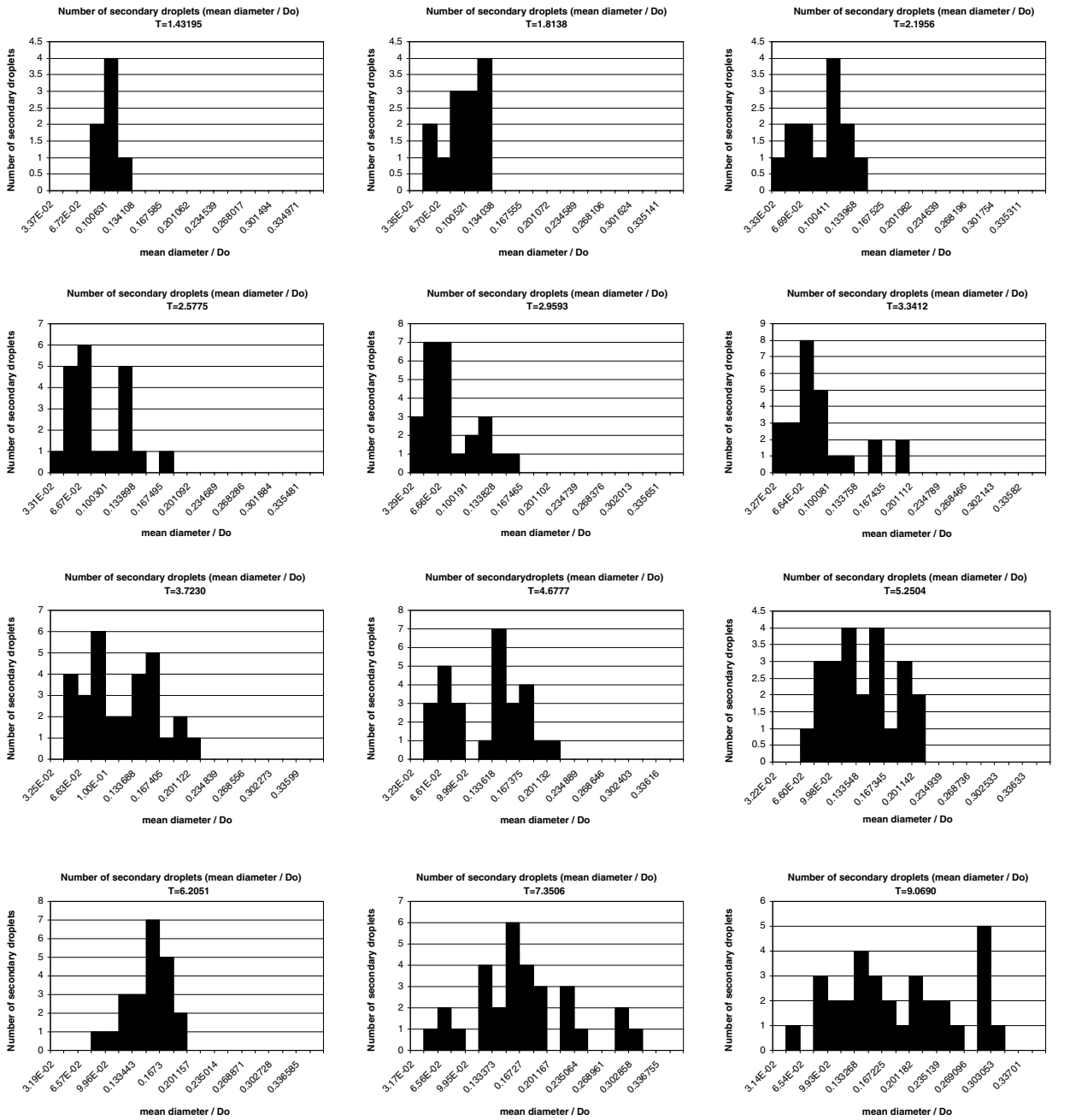

Fig. 13. Distribution of the satellite droplet diameter as a function of time for case C, using three levels of local refinement using three levels of local refinement ($We = 598,\ Re = 17467,\ H = 0.116,\ Fr = 867,$ locref $= 3$).

tion and the second one is in the azimuthal direction, as can be seen in Fig. 8(a) at $T = 5.441$ and as reported also by Cossali et al. [6]. The crown's width is thinner in case C, than in case B, due to the higher We impact number. Under the effect of the perturbations and surface tension, holes are created in the thin crown liquid sheet, as it can be seen in Fig. 8(a), as also verified by the theory of Macklin and Metaxas [5].

Please cite this article in press as: N. Nikolopoulos et al., Three-dimensional numerical investigation of a ..., J. Comput. Phys. (2007), doi:10.1016/j.jcp.2006.12.002

5.1.10. Grid dependency

The time evolution of this case was also predicted, using four levels of local refinement. The numerical investigation predicts crown formation and ''prompt'' splashing, as shown in Fig. 8(b). Thus, the numerics for both grid refinement levels seem to predict ''prompt'' splashing.

In addition Fig. 9 presents also results for the finer mesh of the time evolution of the lamella's dimensions. As far as the lamella's dimensions are concerned, a good agreement between three and four levels of local refinement is found. Nevertheless, for the lamella's height an increase is predicted using four levels of local refinement (less than 20%), due to the more vertical lamella's growth. Moreover, this is combined with a smaller average crown thickness.

In addition, the four levels grid refinement simulation, predicts an earlier rim cusping and jetting, than the corresponding one with three levels of local refinement. More and smaller secondary droplets (68 in contrast to 39, $T = 1.241$, Fig. 11(a) and (b) (locref $= 4$)) are produced. Again the rim's instability creates a number of fingers, which elongate with time and eventually break up to yield the secondary droplets through a Rayleigh instability mechanism as shown in Fig. 11(a) using four levels of grid refinement. Using either three or four levels of local refinement, each secondary droplet diameter is discretized by approximately seven computational cells.

In addition, the predicted initial number of protruding jets around the crown periphery is greater (Fig. 10(a) using four levels of local grid refinement), but this number quickly decreases, due to the merging of the closest jets, during the crown evolution, in accordance with the results of other researchers, like Cossali et al. [6], Yarin and Weiss [2]. Consequently in case C the mesh refinement, as shown by the numerical results, does not really allow to conclude that especially the first droplets breakup is not numerically selected. Specifically, characteristics of splashing (jet elongation, number and size of secondary droplets) quite significantly depend on the level of mesh refinement.

The calculated maximum gas, liquid velocity and pressure at times $T < 0.083$ and $T > 0.193$ take almost the same values for three and four levels of local refinement. However, during the intermediate times ($0.083 < T < 0.193$) the predicted values begin to differ. For example the maximum gas and liquid velocity during this period are approximately 410% and 230%, respectively, of the droplet impact velocity; the maximum pressure value is approximately 336% of the initial droplet kinetic energy, in terms of C_p defined in Section 5.1, at the front stagnation point. These peak values are about 40% higher compared to those obtained with three levels of local refinement.

5.2. Crater dynamics

Following the impact of the droplet on the film, liquid from the film is transferred to the lamella liquid sheet. In particular, the crown's mass consists more from liquid initially forming the wall film than from liquid coming from the droplet, as reported by Nikolopoulos et al. [10] using a two-VOF model. As a result, in the crater the shallow film ($H = 0.116$) becomes even thinner and surface waves develop, as also reported by Weiss and Yarin [1]. For case A at time $T = 2.525$ the minimum film height found at the crown's base, within the crater is equal to 1.98% of the initial droplet diameter, for case B at time $T = 2.839$ is approximately 2.11% of the initial droplet diameter and finally for case C at time $T = 2.959$ is approximately 2.06% of the initial droplet diameter.

The numerical grid using three or four levels of local refinement is not fine enough to discritize the film thickness at these stages. For example in case C using three levels of local refinement at about time $T = 2.959$, the crater's film height is covered by only one computational cell ($dx = D_o/40$), whilst for the same case using four levels of local refinement the film is covered at the same time by two computational cells ($dx = D_o/80$). As a result, spots of triple phase of wall-gas and liquid phase are calculated, starting at the base of the crown. At these spots, the boundary condition of a static contact angle of 60° is activated, leading to the accumulation of liquid mass at certain points on the solid surface and inevitably creating secondary droplets inside the crater, under the simultaneous action of surface tension. Using four levels of local refinement the development of such spots is delayed, since the grid density is higher. Therefore, the formation of secondary droplets inside the crater as it is depicted in Figs. 3(a),

Please cite this article in press as: N. Nikolopoulos et al., Three-dimensional numerical investigation of a ..., J. Comput. Phys. (2007), doi:10.1016/j.jcp.2006.12.002

6(a) and 8(a) is only a numerical artifact, because of the coarse grid in this region, despite the use of adaptive local grid refinement technique.

6. Conclusions

The flow development arising from the normal impingement of a droplet onto a wall film was numerically studied using a finite volume methodology incorporating the volume of fluid (VOF) methodology and utilizing an adaptive local grid refinement technique. Three-dimensional numerical simulations proved to be accurate at acceptable levels, predicting not only the evolution of the formation of the lamella during the initial stages of impact but also the 3-D formation of satellite droplets realized with high impact *We* numbers. Disturbances on the shape and velocity field of the impinging droplet and the film surface are not applied, but are inherently induced during the motion of the droplet prior or during impingement. At the intermediate impact *We* number (case B), between deposition (case A) and splashing (case C) a different mechanism of splashing, not reported in the literature (verified by grid dependency tests), is observed, during which a ring detaches from the crown, deforms to ligaments, and later breaks-up into secondary droplets in a way similar to the Rayleigh instability theory. For higher impact Weber numbers not only at intermediate times of the splashing process, but also in its early stages of development, the Rayleigh instability dominates the spill-off of secondary droplets, while at later stages surface tension effects play a significant role in the break up. The VOF method was capable of predicting the details of the flow field, like air bubble entrapment, capillary waves, and air and liquid jetting.

Finally, the grid dependency test proved that the dynamics of droplet impingement onto a wall-film is grid independent for low *We* numbers (deposition and marginal splashing), whilst the dynamics of splashing and particularly those of fine structure are mesh dependant.

Acknowledgment

The financial support of the EU under Contract No. ENK6-2000-00051 is acknowledged.

References

[1] A.D. Weiss, L.A. Yarin, Single drop impact onto liquid films: neck distortion, jetting, tiny bubble entrainment, and crown formation, J. Fluid. Mech. 385 (1999) 229–254.
[2] A. Yarin, A.D. Weiss, Impact of drops on solid surfaces: self-similar capillary waves, and splashing as a new type of kinematic discontinuity, J. Fluid. Mech. 283 (1995) 141–173.
[3] G.E. Cossali, G. Brunello, A. Coghe, M. Marengo, Impact of a single drop on a liquid film: experimental analysis and comparison with empirical models. Italian Congress of Thermofluid Dynamics UIT, Ferrara, 30 June–2 July, 1999.
[4] Z. Levin, P.V. Hobbs, Splashing of water drops on solid and wetted surfaces: hydrodynamics and charge separation, Phil. Trans. R. Soc. Lond. A 269 (1971) 555–585.
[5] W.C. Macklin, G.J. Metaxas, Splashing of drops on liquid layers, J. Appl. Phys. 47 (1976) 3963–3970.
[6] G.E. Cossali, A. Coghe, M. Marengo, The impact of a single drop on a wetted solid surface, Exp. Fluids 22 (1997) 463–472.
[7] An-Bang Wang, Chi-Chang Chen, Splashing impact of a single drop onto very thin liquid films, Phys. Fluids 12 (9) (2000), Letters.
[8] I.V. Roisman, C. Tropea, Impact of a drop onto a wetted wall: description of crown formation and propagation, J. Fluid Mech. 402 (2002) 373–397.
[9] M.F. Trujillo, C.F. Lee, Modeling crown formation due to the splashing of a droplet, Phys. Fluids 13 (9) (2001).
[10] N. Nikolopoulos, A. Theodorakakos, G. Bergeles, Normal impingement onto a wall film: a numerical investigation, Int. J. Heat Fluid Flow 26 (2005) 119–132.
[11] C. Josserand, S. Zaleski, Droplet splashing on a thin liquid film, Phys. Fluids 15 (6) (2003).
[12] S.T. Thoroddsen, The ejecta sheet generated by the impact of a drop, J. Fluid Mech. 451 (2002) 373–381.
[13] C.D. Stow, M.G. Hadfield, An experimental investigation of fluid flow resulting from the impact of a water drop with an underyielding dry surface, Proc. R. Soc. London A 373 (1981) 419–441.
[14] A.L. Yarin, Free liquid Jets and Films: Hydrodynamics and Rheology, Longman and Wiley & Son, 1993.
[15] Lord Rayleigh, On the instability of jets, Proc. London Math. Soc. 10 (1878) 4–13.
[16] G.I. Taylor, The dynamics of thin sheets of fluid II. Waves on fluid sheets, Proc. R. Soc. Lond. A 253 (1959) 296–312.
[17] M. Rieber, A. Frohn, A numerical study on the mechanism of splashing, Int. J. Heat Fluid Flow 20 (1999) 455–461.
[18] C.W. Hirt, B.D. Nichols, Volume of fluid (VOF) method for the dynamics of free boundaries, J. Comput. Phys. 39 (1981) 201–225.
[19] D. Gueyffier, S. Zaleski, Formation de digitations lors de l'impact d'une gouttesur un film liquide (finger formation during droplet impact on a liquid film), Comptes Rendus Acad. Sci. Paris Ser II 98 (December) (1998).

Please cite this article in press as: N. Nikolopoulos et al., Three-dimensional numerical investigation of a ..., J. Comput. Phys. (2007), doi:10.1016/j.jcp.2006.12.002

[20] R.D. Richtmyer, Taylor instability in shock acceleration of compressible fluids, Comm. Pure Appl. Math. 8 (1960) 297–319.
[21] C. Arcoumanis, M. Gavaises, B. French, Effect of fuel injection processes on the structure of diesel sprays, SAE Paper 970799, SAE Transactions, 1997.
[22] C. Bai, A.D. Gosman, Development of methodology for spray impingement simulation, Soc. Automot. Eng. 950283 (1995).
[23] D. Morton, M. Rudman, L. Jong-Leng, An investigation of the flow regimes resulting from splashing drops, Phys. Fluids 12 (4) (2000) 747–763.
[24] D.W. Stanton, C.J. Rutland, Multi-dimensional modeling of thin liquid films and spray-wall interactions resulting from impinging sprays, Int. J. Heat Mass Transfer 41 (1998) 3037–3054.
[25] C. Tropea, M. Marengo, The impact of drops on walls and films, in: Third International Conference on Multiphase Flow, ICMF '98 Lyon France, 1998, June 8–12.
[26] A. Theodorakakos, G. Bergeles, Simulation of sharp gas–liquid interface using VOF method and adaptive grid local refinement around the interface, Int. J. Numer. Meth. Fluids 45 (2004) 421–439.
[27] S.V. Patankar, D.B. Spalding, A calculation procedure for heat, mass and momentum transfer in three dimensional parabolic flows, Int. J. Heat Mass Transfer 15 (1972) 1787–1806.
[28] C.M. Rhie, W.L. Chow, A numerical study of the turbulent flow past an isolated airfoil with trailing edge separation, AIAA J. 21 (1983) 1525–1532.
[29] O. Ubbink, R.I. Issa, A method for capturing sharp fluid interfaces on arbitrary meshes, J. Comput. Phys. 153 (1) (1999) 26–50.
[30] H. Jasak, Error analysis and estimation for finite volume method with applications to fluid flows. Ph.D thesis, Department of Mechanical Engineering, Imperial College of Science, Technology and Medicine, University of London, 1996.
[31] N.H. Oguz, A. Prosperetti, Bubble entrainment by the impact of drops on liquid surfaces, J. Fluid Mech. 219 (1990) 143–179.
[32] Z.-Nu Wu, Approximate critical *We* number for the breakup of an expanding torus, Acta Mech. 166 (2003) 231–239.

Please cite this article in press as: N. Nikolopoulos et al., Three-dimensional numerical investigation of a ..., J. Comput. Phys. (2007), doi:10.1016/j.jcp.2006.12.002